# Experimental Study of Sliding Base-Isolated Buildings with Magnetorheological Dampers in Near-Fault Earthquakes

Sanjay Sahasrabudhe, M.ASCE,[1] and Satish Nagarajaiah, M.ASCE[2]

**Abstract:** The increase in bearing displacements of sliding isolated buildings due to near-fault earthquakes, with long-period pulse type of ground motion, is an important problem. Often, supplemental nonlinear passive dampers are incorporated into the isolation system to reduce the base displacements; however, this may increase the interstory drifts and accelerations in the superstructure. Hence, there is a need to examine whether controllable nonlinear dampers can reduce the base displacements without a further increase in superstructure response. In this study, the effectiveness of variable damping, provided by magnetorheological (MR) dampers, in reducing the response of sliding isolated buildings during near-fault earthquakes is investigated using a 1:5 scale steel two-story model. A nonlinear analytical model is developed with due consideration given to the nonlinearities of the friction bearings and the MR damper. A Lyapunov-based control algorithm is developed for control of the MR damper and the building model, and tested on a shake table. Results of passive low/high damping cases and semiactive cases are compared. It is shown that the variable damping reduces base displacements and superstructure responses further than passive low/high damping cases.

**DOI:** 10.1061/(ASCE)0733-9445(2005)131:7(1025)

**CE Database subject headings:** Base isolation; Damping; Earthquakes; Ground motion; Displacement; Superstructures; Structural response.

## Introduction

Seismic isolation is a widely accepted technique (Kelly 1997) for protecting buildings and bridges from strong earthquakes. Recently recorded response of USC hospital base-isolated building (Nagarajaiah and Sun 2000) during the 1994 Northridge earthquake has shown the effectiveness of seismic isolation; the elastomeric bearings yielded and dissipated energy and the superstructure remained elastic during the earthquake, as designed. Similarly base isolated buildings which experienced the 1995 Kobe earthquake behaved as designed (Naeim and Kelly 1999). However, near-fault earthquakes with large amplitude, long period, and pulse type of excitation tend to produce large base displacements in base-isolated buildings. If the seismic gap is inadequate to accommodate such large base displacements, then the resulting impact response can be undesirable (Hall et al. 1995; Nagarajaiah and Sun 2001). Supplemental nonlinear passive dampers have been incorporated into the isolation system (Asher et al. 1996; Makris and Chang 2000) to reduce the base displacements in near-fault earthquakes. Although, supplemental dampers certainly reduce the base displacements, they may increase the interstory drifts and accelerations in the superstructure (Kelly 1999). It is to be noted that despite the susceptibility of base-isolated buildings to near-fault earthquakes, their performance is still superior to that of the fixed base case provided the large base displacements are allowable. There is a need to examine whether controllable nonlinear dampers, which can vary their damping based on feedback control, can reduce base displacements without increasing the superstructure response. There are varieties of controllable dampers available (Symans and Constantinou 1999; Spencer and Nagarajaiah 2003) for such applications.

Recently, several researchers have investigated the application of semiactive dampers (Sahasrabudhe and Nagarajaiah 2005; Narasimhan and Nagarajaiah 2005). The application of controllable magnetorheological (MR) fluid dampers (Carlson and Chrzan 1994; Spencer et al. 1997) in smart elastomeric base-isolated buildings has been studied analytically (Nagarajaiah 1994; Ramallo et al. 2002) and experimentally (Yoshioka et al. 2002); they have shown that MR dampers, controlled using a modified clipped optimal control algorithm, can be very effective and that their adaptability is particularly suited for wide range of ground motion intensities and characteristics. The application of controllable electrorheological dampers for response control of elastomeric base-isolated buildings was originally studied by Makris (1997), followed by Gavin (2001) and shown to be effective in reducing response. Semiactive friction dampers (Yang and Agrawal 2002), and tuned interaction dampers (Zhang and Iwan 2002) have also been shown to be effective for response control of elastomeric base-isolated buildings, analytically. Variable orifice fluid dampers (Kurata et al. 1999; Symans and Kelly 1999) have been applied for reducing the lateral-torsional response of elastomeric base isolated buildings, and studied analytically by Gavin et al. (2003); the study found the dampers to be effective. Response control of sliding isolated buildings using variable ori-

[1]Structural Engineering Dept., J. Ray McDermott Engineering, LCC, Houston, TX 77079; formerly, Postdoctoral Researcher, Dept. of Civil Engineering, Rice Univ., Houston, TX 77005.

[2]Associate Professor, Depts. of Civil & Environmental Engineering & Mechanical Engineering/Material Science, Rice Univ., Houston, TX 77005. E-mail: nagaraja@rice.edu

Note. Associate Editor: Sashi K. Kunnath. Discussion open until December 1, 2005. Separate discussions must be submitted for individual papers. To extend the closing date by one month, a written request must be filed with the ASCE Managing Editor. The manuscript for this paper was submitted for review and possible publication on May 27, 2004; approved on December 20, 2004. This paper is part of the ***Journal of Structural Engineering***, Vol. 131, No. 7, July 1, 2005. ©ASCE, ISSN 0733-9445/2005/7-1025–1034/$25.00.

fice dampers has been studied experimentally by Madden et al. (2002). They have shown that experimental performance of their adaptive isolation system was not significantly different from that of the passive isolation system. Although, their analytical study (Madden et al. 2003) showed that the adaptive isolation system was capable of simultaneously limiting both the response of the isolation system and the superstructure in cases that they studied. Madden et al. (2002) concluded that more experimental work is needed to address some of the limitations of their study. Hence, there is a need to investigate experimentally the effectiveness of controllable dampers in sliding isolated buildings in near-fault earthquakes, which is the focus of the current study.

The comprehensive (Sahasrabudhe 2002) analytical and experimental results of the study of a two-story sliding isolated building with a sliding isolation system and a MR damper is presented in this paper. The initial experimental findings of the study (which began in 1999) were reported by Sahasrabudhe et al. (2000). The responses to near-fault earthquakes are computed using a nonlinear analytical model developed in this study and compared with recorded responses from the shake table tests on a 1:5 scale model. Results of passive low and high damping cases are compared with that of the semiactive case. It is shown that the variable MR damper improves the performance significantly in the earthquakes considered in this study.

## Magnetorheological Damper

The damper (developed by Lord Corporation, North Carolina) consists of MR fluid in the main cylinder as shown in Fig. 1(a). Micron-sized iron particles are suspended in silicon fluid forming the MR fluid. The piston has an annular orifice and a magnetic coil. An accumulator is provided at the end of the damper to prevent cavitations in the fluid. The damper is 15.2 cm (6.00 in.) long in the compressed position and the main cylinder is 4.2 cm (1.65 in.) in diameter. The damper has a 5.7 cm (2.25 in.) stroke. The damper is capable of withstanding temperatures between 130 and −40°C. The voltage supplied to the damper varies from 0 to 4 V. When the damper is stroked, fluid passes through the annular orifice which is surrounded by a coil. As the voltage signal is supplied, the magnetic field in the coil changes. The iron particles suspended in the MR fluid line up and form chains under the magnetic field. The fluid changes from freely flowing viscous fluid to semisolid. Due to this phenomenon, force in the MR damper increases. Response time for this phenomenon is less than 25 ms, thus making it a suitable device for seismic applications (Spencer et al. 1997). Fig. 1(b) shows the experimental results of the test conducted with harmonic excitation of 2.5 Hz. The damper was tested with varying voltage from 0 to 4 V. The force—displacement response shown in Fig. 1(b) demonstrates the variable nonlinear damping behavior of the MR damper. Force in the MR damper increases with voltage from around 220 N (50 lb) at 0 V to around 1350 N (300 lb) at 4 V. The loops are stable and repeatable over a large number of cycles.

## 1:5 Scale Sliding Isolated Building with Magnetorheological Damper

A 1:5 scale two-story building model was designed (Sahasrabudhe et al. 2000) and built based on artificial mass simulation (Mills et al. 1979) as shown in Figs. 2–4, and Table 1. Fig. 3 shows the sliding isolated building model connected to the shake

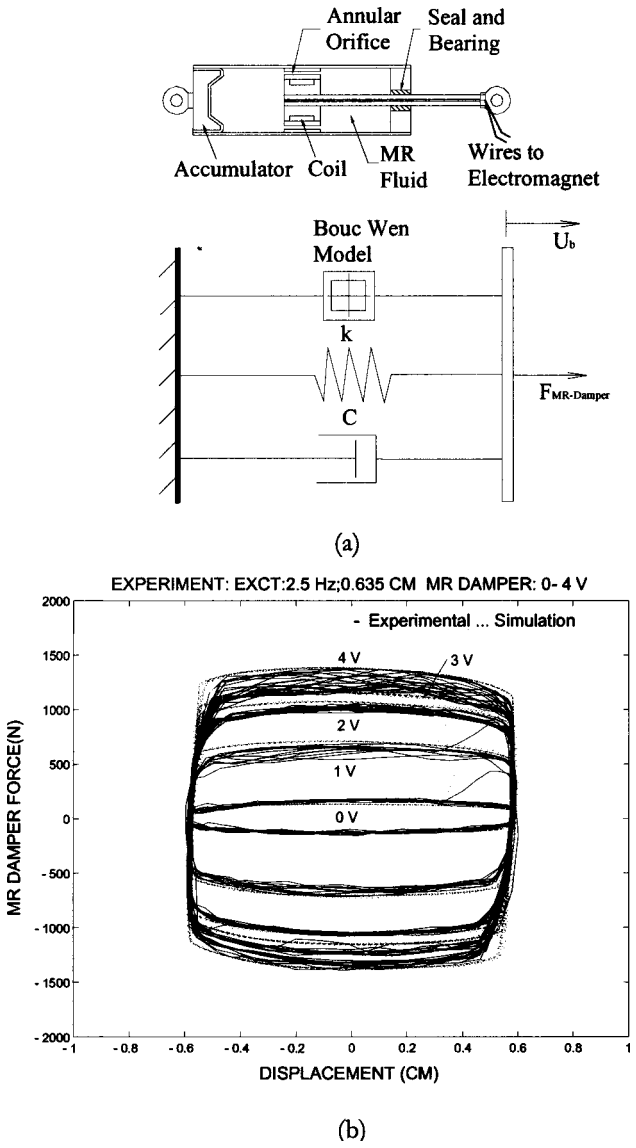


**Fig. 1.** (a) Schematics of magnetorheological damper and analytical model; and (b) experimental and analytical force-displacement response to harmonic excitation of 2.5 Hz

table and reference instrumentation frame to the right. Fig. 4 shows the close-up view of the sliding bearings, MR damper, and restoring springs connected between the base and the shake table. Weight of each floor is 5.8 kN. Weight of the base is 5.44 kN. The length of the building is 1.47 m, the height is 1.48 m, and the width is 0.74 m. At model scale, the building is designed to have natural period of 0.9 s in the isolated case and 0.15 s in the nonisolated case, which is 2 s and 0.34 s, respectively, at proto-

**Table 1.** Scaling Factors

| Parameter | Scaling factors | 1:5 model |
|---|---|---|
| Length | $l_r$ | 1/5 |
| Time | $\sqrt{l_r}$ | $1/\sqrt{5}$ |
| Displacement | $l_r$ | 1/5 |
| Velocity | $\sqrt{l_r}$ | $1/\sqrt{5}$ |
| Acceleration | 1 | 1 |
| Force | $l_r^2$ | 1/25 |

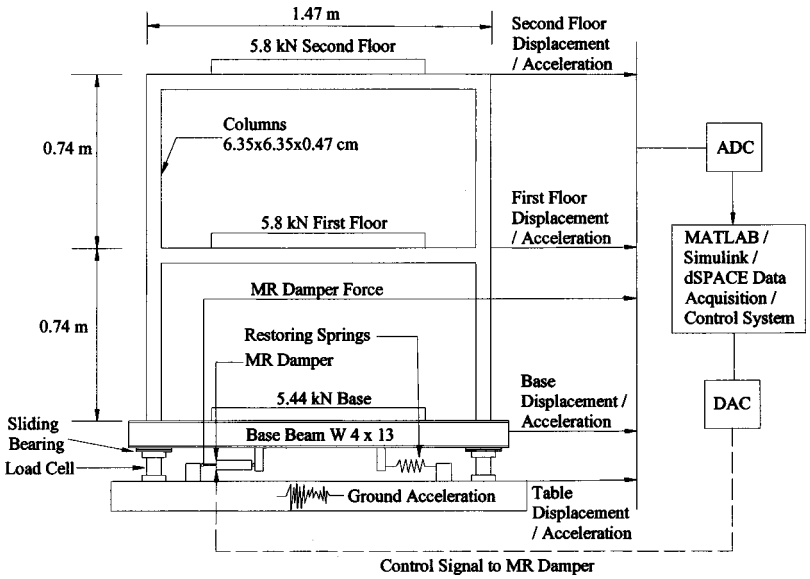


**Fig. 2.** Sliding isolated building model with magnetorheological damper and block diagram of data acquisition and controller

type scale. The building model has four sliding isolated bearings, consisting of a Teflon®-stainless steel interface (Fig. 4). The sliding bearings are supported by triaxial load cells, which measure frictional forces transmitted from base to the shake table (Fig. 4). The measured frictional force normalized with respect to the weight of the building as a function of the relative base displacement is shown in Fig. 5(a). The coefficient of friction varies with velocity, from 0.06 at low velocity to 0.13 at high velocity as shown in Fig. 5(b). Restoring springs having 720 N/cm stiffness and the MR damper are connected between the base of the building and the shaking table as shown in Fig. 4. A load cell of capacity 4.45 kN is used to measure forces in the MR damper. The building model is instrumented with linear variable differential transducers and accelerometers at base, first, and second floor to measure displacement and acceleration response. Data acquisition and control is performed using a dSPACE system with *MATLAB/Simulink*. The block diagram of data acquisition and control system is shown in Fig. 2.

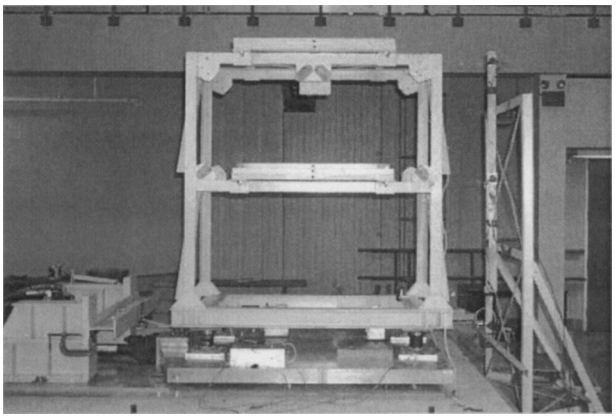

**Fig. 3.** Two-story sliding isolated building model on the shaking table shown without the base weight

### *Earthquake Excitations*

The response of the sliding isolated building model in several near-fault earthquakes is studied. The study includes: (1) MR damper off—constant 0 V—with passive low damping (equivalent linear damping ratio of ~6%), (2) MR damper on—constant 4 V—with passive high damping (equivalent linear damping ratio of ~45%) and, (3) controlled case in which the voltage is switched between low and high damping levels based on the control algorithm. The following earthquakes are considered in this study.

1. El-Centro Earthquake (May 18, 1940): Station name: Imperial Valley Irrigation District, NS component, peak acceleration: 0.37 g.
2. Northridge Earthquake (January 17, 1994): Station name: Newhall-LA County Fire Station, Station No. 24279, Channel 1-90° component, peak acceleration: 0.608 g.
3. Northridge Earthquake (January 17, 1994): Station Name: Sylmar County Hospital Parking Lot, Station No. 24514, Channel 1-90° component, peak acceleration: 0.461 g.
4. Hyogo-ken Nanbu (Kobe) Earthquake (January 17, 1995): Station Name: Kobe Japanese Meteorological Agency, NS component, peak acceleration: 0.816 g.

Shake table tests are performed for three chosen earthquakes

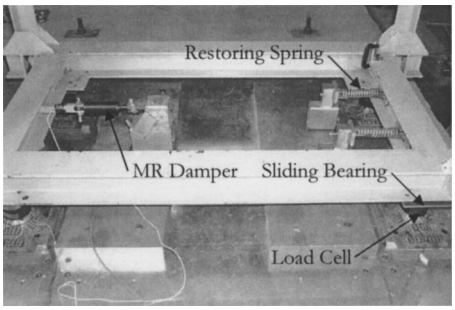


**Fig. 4.** Sliding bearings, magnetorheological damper and restoring springs connected between base and shake table

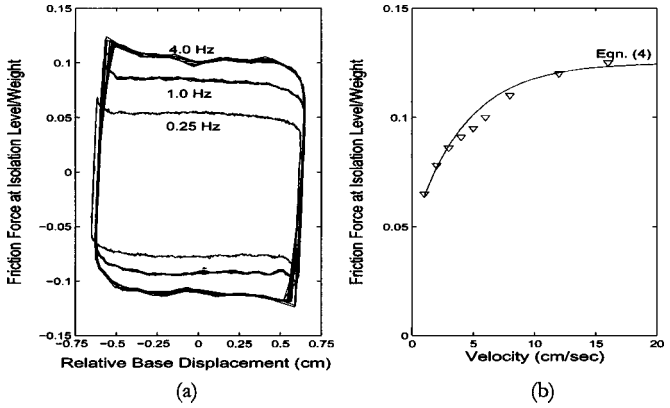


**Fig. 5.** (a) Measured friction force in the isolators/weight versus displacement; and (b) variation of friction force/weight as a function of velocity

namely, El Centro, Newhall 90, and Sylmar 90. The El Centro earthquake exhibits characteristics of far-field ground motions although it was recorded near fault. Additionally fault normal cases of Newhall, Sylmar, and Kobe earthquake were also studied; the results of which are presented in Sahasrabudhe (2002). As per Table 1, the earthquake signals were compressed by a time scale factor of $1/\sqrt{5}$.

## Analytical Model

The analytical model of the smart sliding isolated building model accounts for the nonlinear characteristics of the frictional elements and the MR damper. Mass of first floor and second floor is 5.92 N s$^2$/cm. Mass of the base is 5.54 N s$^2$/cm. Springs with total stiffness of 720 N/cm were connected between base of the building and shake table. The equations of motion are:

$$M_2\ddot{U}_2 + C_2(\dot{U}_2 - \dot{U}_1) + K_2(U_2 - U_1) = -M_2\ddot{U}_g \tag{1}$$

$$M_1\ddot{U}_1 + C_1(\dot{U}_1 - \dot{U}_b) + K_1(U_1 - U_b) - C_2(\dot{U}_2 - \dot{U}_1) - K_2(U_2 - U_1) = -M_1\ddot{U}_g \tag{2}$$

$$M_b\ddot{U}_b + \sum_{i=1}^{4} F_{bi} + F_{\text{MR-Damper}} + K_bU_b - C_1(\dot{U}_1 - \dot{U}_b) - K_1(U_1 - U_b) = -M_b\ddot{U}_g \tag{3}$$

where degrees of freedom are base displacement with respect to shake table, $U_b$, first floor displacement with respect to shake table, $U_1$, and second floor displacement with respect to shake table, $U_2$. $\ddot{U}_g$=ground acceleration. $\ddot{U}_b, \ddot{U}_1, \ddot{U}_2$=base, first floor, and second floor acceleration, respectively. $M_b, M_1, M_2$=base, first floor, and second floor masses, respectively. $K_1$=first story stiffness; $K_2$=second story stiffness; and $K_b$=base spring stiffness. $C_1$=the first-story damping coefficient; and $C_2$=second-story damping coefficient. $F_{bi}$=friction forces in the sliding bearings. $F_{\text{MR-Damper}}$=force generated by the MR damper.

The force in sliding bearings $f_s = \Sigma_{i=1}^{4} F_{bi}$, where $F_{bi} = \mu_i w_i z_i$ with $\mu_i$=coefficient of friction at bearing at location $i$, $w_i$=normal load on bearing at location $i$, $z_i$ is the Wen's (1976) hysterisis parameter used to model friction [Eq. (5)]. The coefficient of friction (Nagarajaiah et al. 1991a,b; 1993) at bearing at location $i$ is given by

$$\mu_i = f_{\max\_i} - (f_{\max\_i} - f_{\min\_i})e^{-(a_i abs(\dot{U}_b))} \tag{4}$$

where $f_{\max\_i}=0.13$, $f_{\min\_i}=0.06$, $a_i=0.2362$ s/cm.
The Wen's hysteresis variable $z$ is obtained by the following equation (with $Y_i=0.127$ cm—small yield displacement of Teflon® before sliding, $\gamma=0.9$, $\beta=0.1$)

$$Y_i\dot{z}_i + \gamma|\dot{U}_b|z_i|z_i| + \beta\dot{U}_b z_i^2 - \dot{U}_b = 0 \tag{5}$$

From analytical model shown in Fig. 1(a), $F_{\text{MR-Damper}}$ is given as

$$f_c = F_{\text{MR-Damper}} = (\alpha z)f(v) + C\dot{U}_b + kU_b \tag{6}$$

where $k=8.24$ N/cm, $\alpha=(66.9+258.6v)$ N, $C=(7.2+5.87v)$ N s/cm, nondimensional parameter $f(v)=\beta_3v^3-\beta_2v^2+\beta_1v+\beta_0$ (where $\beta_0=0.8133$, $\beta_1=1.3706$, $\beta_2=0.6679$, and $\beta_3=0.0808$, with appropriate dimensions) with voltage supplied to the MR damper being $v$. The best-fit parameters were determined based on harmonic test results of the MR damper. The hysteresis variable $z$ for the MR damper is obtained by solving another equation identical to Eq. (5) with $Y_i=0.165$ cm.

The corresponding state equation, measured output equation, and regulated output equation are as follows:

$$\dot{\mathbf{x}}(t) = \mathbf{A}\mathbf{x}(t) + \mathbf{B}f_c(t) + \mathbf{B}f_s(t) + \mathbf{E}\ddot{U}_g(t) \tag{7}$$

$$\mathbf{y}(t) = \mathbf{C_m}\mathbf{x}(t) + \mathbf{D_m}f_c(t) + \mathbf{D_m}f_s(t) + \mathbf{E_m}\ddot{U}_g(t) \tag{8}$$

$$\mathbf{z}(t) = \mathbf{C_z}\mathbf{x}(t) + \mathbf{D_z}f_c(t) + \mathbf{D_z}f_s(t) + \mathbf{E_z}\ddot{U}_g(t) \tag{9}$$

where

$$\mathbf{A} = \begin{bmatrix} 0 & 1 \\ -\mathbf{m}^{-1}\mathbf{k} & -\mathbf{m}^{-1}\mathbf{c} \end{bmatrix}, \quad \mathbf{B} = \begin{Bmatrix} 0 \\ \mathbf{m}^{-1} \end{Bmatrix}, \quad \mathbf{E} = \begin{Bmatrix} 0 \\ -1 \end{Bmatrix}$$

and, $\mathbf{C_m}, \mathbf{C_z}, \mathbf{D_m}, \mathbf{D_z}, \mathbf{E_m}, \mathbf{E_z}, \dot{\mathbf{x}}(t), \mathbf{x}(t), \mathbf{y}(t), \mathbf{z}(t)$=appropriately defined system matrices or vectors. The measured outputs are absolute accelerations at all floors and the base. The measured accelerations can be passed through second-order filter (Spencer et al. 1998) to obtain absolute velocities and displacements.

The equations of motion [Eqs. (1)–(3)] are solved using an iterative method (Nagarajaiah et al. 1991a,b). The algorithm involves the solution of equations of motion using the unconditionally stable Newmark's constant-average acceleration method. The solution of differential equations governing the behavior of the nonlinear isolation elements [Eq. (5)] and the MR damper [Eq. (6) together with another equation identical to Eq. (5)] is obtained using the unconditionally stable semi-implicit Runge–Kutta method. The nonlinear forces are moved to the right-hand side as pseudo-forces and an iterative procedure consisting of corrective pseudo-forces is employed within each time step until equilibrium is achieved.

## Control Algorithm

The control algorithm is described as follows. Since the base-isolated structures respond primarily in the first mode, the superstructure is assumed to be rigid. Thus the equations of motion reduce to

$$m\ddot{u}_a + k_b(u_a - u_g) + f_s + f_c = 0 \tag{10}$$

where $m$=total mass; $k=k_b$=base spring stiffness, $u_a$=absolute displacement; $u_g$=ground displacement; and $f_c=c_v\dot{u}_b$, with $u_b=u_a-u_g$. Rewriting Eq. (10)

$$\ddot{u}_a = -\frac{k}{m}(u_a - u_g) - \frac{f_s}{m} - \frac{f_c}{m} \tag{11}$$

which can be formulated in state space

$$\begin{Bmatrix} \dot{u}_{1a} \\ \dot{u}_{2a} \end{Bmatrix} = \begin{Bmatrix} \dot{u}_a \\ \ddot{u}_a \end{Bmatrix} = \begin{bmatrix} 0 & 1 \\ -\frac{k}{m} & 0 \end{bmatrix} \begin{Bmatrix} u_a \\ \dot{u}_a \end{Bmatrix} - \begin{Bmatrix} 0 \\ \frac{1}{m} \end{Bmatrix} f_s - \begin{Bmatrix} 0 \\ \frac{1}{m} \end{Bmatrix} f_c + \begin{Bmatrix} 0 \\ \frac{1}{m} \end{Bmatrix} k_b u_g \tag{12}$$

Thus, Eq. (12) can be written as

$$\dot{\mathbf{U}}_a = \mathbf{A}U_a + \mathbf{B}f_s + \mathbf{B}f_c + \mathbf{B}k_b u_g \tag{13}$$

where

$$\mathbf{A} = \begin{bmatrix} 0 & 1 \\ -\frac{k}{m} & 0 \end{bmatrix}, \quad \mathbf{B} = \begin{Bmatrix} 0 \\ \frac{1}{m} \end{Bmatrix}$$

The Lyapunov function $V$ is defined as:

$$V = \frac{1}{2}\sigma^T(\mathbf{U}_a)\sigma(\mathbf{U}_a) \tag{14}$$

where

$$\sigma(\mathbf{U}_a) = \mathbf{P}^T\mathbf{U}_a = [P_1 \quad P_2]\begin{Bmatrix} u_a \\ \dot{u}_a \end{Bmatrix} \tag{15}$$

Choosing $P_1=\sqrt{k}$ and $P_2=\sqrt{m}$ yields $V=\frac{1}{2}ku_a^2+\sqrt{k}\sqrt{m}u_a\dot{u}_a+\frac{1}{2}m\dot{u}_a^2$, where the first term represents the total strain energy in the spring, the second term represents the total dissipated energy, and the third term represents the total kinetic energy

$$\dot{V} = \sigma^T(U_a)\dot{\sigma}(U_a) = U_a^T P P^T \dot{U}_a \tag{16}$$

Simplifying Eq. (16), we get

$$\dot{V} = \sigma^T(U_a)P^T B\dot{u}_b\left(-c_v + \frac{1}{\dot{u}_b}\left(\frac{m}{p_2}P_1\dot{u}_a - ku_b - f_s\right)\right) \tag{17}$$

Since only $c_v$ can be varied for $\dot{V}$ to be negative or minimum

$$c_v = \begin{cases} C_{\max} & \sigma^T(U_a)P^T B\dot{u}_b > 0 \\ 0 \text{ or } C_{\min} & \sigma^T(U_a)P^T B\dot{u}_b < 0 \end{cases} \tag{18}$$

$$c_v = \begin{cases} C_{\max} & \frac{P_2}{m}(P_1u_a + P_2\dot{u}_a)\dot{u}_b > 0 \\ 0 \text{ or } C_{\min} & \frac{P_2}{m}(P_1u_a + P_2\dot{u}_a)\dot{u}_b < 0 \end{cases} \tag{19}$$

Substituting $P_1=\sqrt{k}$ and $P_2=\sqrt{m}$ leads to

$$c_v = \begin{cases} C_{\max} & (\omega_n u_a + \dot{u}_a)\dot{u}_b > 0 \\ 0 \text{ or } C_{\min} & (\omega_n u_a + \dot{u}_a)\dot{u}_b < 0 \end{cases} \tag{20}$$

where $c_v$=variable damping coefficient of the MR damper; $C_{\min}$=minimum damping coefficient for 1 Volt; and $C_{\max}$=maximum damping coefficient for 4 V. Analytical study lead to the introduction of a nondimensional constant $\alpha=14.3$ ($\omega_n=7$ rad/s) for optimal response reduction, i.e. $(\alpha\omega_n u_a+\dot{u}_a)\dot{u}_b$ being the condition to check with $P_1=100$ and $P_2=1$.

An additional point to note is that since the absolute displacement and velocity are needed in Eq. (20), they can be obtained from measured absolute acceleration. The absolute displacement can be obtained using integrators/filters proposed by Spencer et al. (1998). The comparison of experimental and filtered absolute velocity and displacement under time scaled Sylmar 90 excitation is shown in Fig. 6. It is evident that the filtered absolute velocity and absolute displacement is in good agreement with the recorded velocity and displacement. Note that in Fig. 6 a 0.01 s time shift is introduced in the absolute velocity and displacement time history.

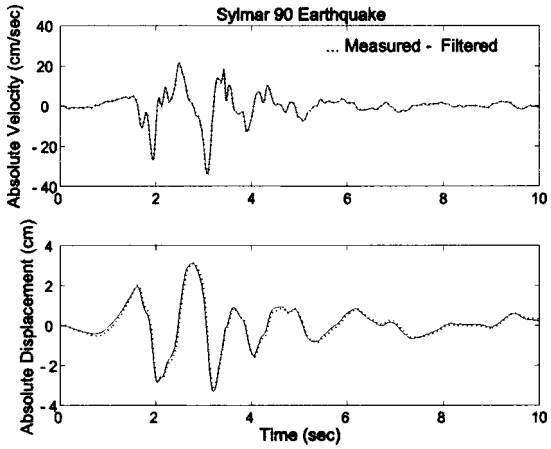


**Fig. 6.** Comparison of experimental and filtered absolute velocity and displacement time history response under Sylmar 90 earthquake

## Results

Results of analytical simulations and shake table experiments are presented in Table 2. The percentage of reductions in the controlled case and passive high damping case, as compared to passive low damping case, are shown in brackets in Table 2. In particular, reductions in (1) Newhall 90, (2) Sylmar 90, and (3) El Centro are notable. To highlight these reductions, results are presented in Figs. 7 and 8. The peak relative base displacement response and peak total force at the isolation level (total force–friction force, MR damper force, and spring force–normalized by total weight) as a function of peak ground acceleration are shown in Figs. 7 and 8, for passive low, passive high, and semiactive damping cases. As evident from Figs. 7 and 8, in Newhall 90, the base displacement is reduced by 16% in the passive high damping case when compared to the passive low damping case. This occurs due to increased energy dissipation in the passive high damping case, with a corresponding 31% increase in total force when compared to the passive low damping case. In the controlled case with semiactive damping, shown in Figs. 7 and 8, the base displacement is reduced by 26% when compared to the passive low damping case, and by 13% when compared to the passive high damping case, while the total force at the isolation level is 14% less than that in the passive high damping case. Thus, the controlled case offers further reductions in base displacements with less energy dissipated (but more efficiently dissipated). A similar set of results are obtained in the analytical study as well (see Table 2). The controlled case reduces the base displacement fur-

**Table 2.** Peak Responses of Two-Story Sliding Isolated Model with Magnetorheological (MR) Damper and Restoring Springs

| | | Relative base displacement (cm) | | Total force at isolation level/weight | | Base acceleration (g) | | First floor acceleration (g) | | Second floor acceleration (g) | | First story drift (cm) | | Second story drift (cm) | |
|---|---|---|---|---|---|---|---|---|---|---|---|---|---|---|---|
| Earthquake | MR | Expt. | Analy. | Expt. | Analy. | Expt. | Analy. | Expt. | Analy. | Expt. | Analy. | Expt. | Analy. | Expt. | Analy |
| Sylmar 90 | 0.0 V | 2.179 | 2.293 | 0.212 | 0.224 | 0.380 | 0.296 | 0.384 | 0.478 | 0.333 | 0.480 | 0.113 | 0.109 | 0.127 | 0.143 |
| Sylmar 90 | 4.0 V | 1.761 (−19%) | 1.649 (−28%) | 0.280 (32%) | 0.263 (17%) | 0.430 (13%) | 0.324 (9%) | 0.482 (25%) | 0.576 (20%) | 0.435 (31%) | 0.550 (15%) | 0.139 (23%) | 0.144 (32%) | 0.147 (16%) | 0.181 (27%) |
| Sylmar 90 | Cont. | 1.409 (−35%) | 1.484 (−35%) | 0.260 (23%) | 0.267 (19%) | 0.400 (5%) | 0.320 (8%) | 0.481 (25%) | 0.515 (8%) | 0.412 (24%) | 0.510 (6%) | 0.128 (13%) | 0.126 (16%) | 0.141 (11%) | 0.157 (10%) |
| Newhall 90 | 0.0 V | 1.914 | 1.815 | 0.214 | 0.210 | 0.420 | 0.260 | 0.484 | 0.551 | 0.359 | 0.560 | 0.123 | 0.129 | 0.122 | 0.162 |
| Newhall 90 | 4.0 V | 1.613 (−16%) | 1.614 (−11%) | 0.280 (31%) | 0.280 (33%) | 0.565 (35%) | 0.300 (15%) | 0.544 (12%) | 0.785 (42%) | 0.590 (64%) | 0.750 (34%) | 0.185 (50%) | 0.155 (20%) | 0.192 (57%) | 0.222 (37%) |
| Newhall 90 | Cont. | 1.411 (−26%) | 1.276 (−30%) | 0.241 (13%) | 0.261 (24%) | 0.580 (38%) | 0.440 (69%) | 0.762 (57%) | 0.774 (40%) | 0.609 (70%) | 0.730 (30%) | 0.163 (35%) | 0.141 (9%) | 0.159 (30%) | 0.209 (29%) |
| El Centro | 0.0 V | 0.969 | 0.938 | 0.166 | 0.160 | 0.440 | 0.192 | 0.301 | 0.497 | 0.352 | 0.450 | 0.098 | 0.111 | 0.142 | 0.150 |
| El Centro | 4.0 V | 0.928 (−4%) | 0.647 (−31%) | 0.246 (48%) | 0.244 (53%) | 0.400 (−9%) | 0.308 (60%) | 0.364 (21%) | 0.541 (9%) | 0.660 (88%) | 0.760 (69%) | 0.131 (34%) | 0.136 (22%) | 0.159 (12%) | 0.166 (11%) |
| El Centro | Cont. | 0.743 (−23%) | 0.775 (−17%) | 0.240 (45%) | 0.243 (52%) | 0.380 (−14%) | 0.282 (47%) | 0.344 (14%) | 0.542 (9%) | 0.690 (96%) | 0.800 (78%) | 0.119 (21%) | 0.136 (22%) | 0.142 (0%) | 0.166 (11%) |

Note: percentage reductions over the 0 V case are shown in brackets. Expt.=experimental; Analy.=analytical; and Cont.=control.




**Fig. 7.** Comparison of experimental peak relative base displacement for two-story model under various conditions

ther than both passive low and high damping cases, with the isolation level forces bounded by the two passive cases. Such reductions in base displacements, as well as forces, reveal the potential of controllable damping. Another interesting feature in Fig. 8 is that as the excitation gets stronger the semiactive case reduces the isolation force further.

Table 2 shows the comparison of the peak interstory drift response and the peak base, first floor, and second floor accelerations under Newhall 90 earthquake with passive low, passive high, and semi-active controlled damping cases. The controlled case maintains the drifts and accelerations within bounds of the two passive cases or at the same level as the passive high damping case.

Experimental responses to Sylmar 90 and El Centro earthquakes are also presented in Figs. 7 and 8 and Table 2. The semiactive control case gives a 35% reduction in base displacement for Sylmar 90 case, and a 23% reduction in base displacement in El Centro case, yet maintaining the total force at isolation level at the same level as the passive high damping case. It is evident from Table 2 that the control case maintains the interstory drifts and accelerations within bounds of the passive cases.

The responses from shake table tests are presented in Figs. 9–14 in the form of relative displacement time history response, total force at isolation level versus relative base-ground displace-




**Fig. 8.** Comparison of experimental peak total shear force at the isolation level for two-story model under various conditions

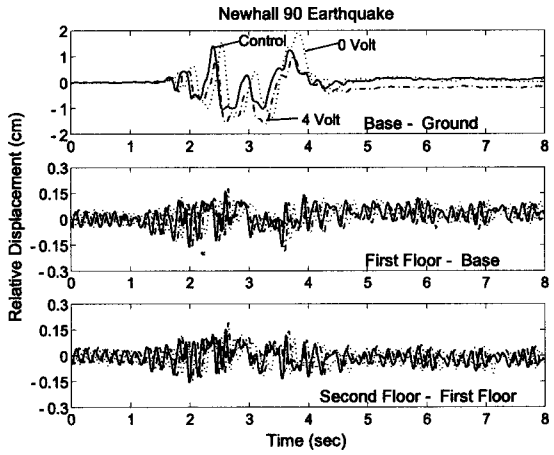


**Fig. 9.** Comparison of experimental displacement response under Newhall 90 excitation

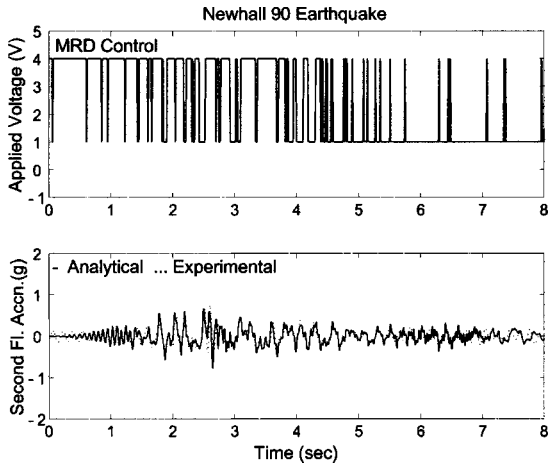


**Fig. 11.** Magnetorheological damper switching and comparison of analytical and experimental second floor acceleration time history response for Newhall 90 earthquake

ment response, applied voltage time history, and second floor acceleration time history response for Newhall 90 and Sylmar 90 excitations. Note that in Figs. 9 and 12 a 0.05 s time shift is introduced in the comparison of relative displacement time histories to hightlight differences clearly. Figs. 10–14 also show the corresponding analytical results. From the comparisons of relative displacement time histories for Newhall 90 presented in Fig. 9, substantial reductions are evident. Most of the displacement occurs at the isolation level and the interstory drifts are significantly reduced. Comparison of total force-base displacement loops for Newhall 90 are presented in Fig. 10. The following features are evident in Fig. 10: (1) The energy dissipation in the passive high damping case is increased; (2) in the semiactive case, the changing width of the force-displacement loop, shown in Fig. 10(c), clearly indicates the adaptive nature of the MR damper system, which leads to more efficient energy dissipation; and (3) the adaptable nature of MR damper reduces both the relative displacement and total forces when compared to the passive systems (see Table 2, also). MR damper switching time history from the experiment and comparison of analytical and experimental second floor acceleration time histories are presented in Fig. 11. A similar set of observations can be made from the Sylmar 90 response plots as well (Figs. 12–14). It is also evident from the peak values of responses presented in Table 2 and Figs. 10, 11, 13, and 14 that the proposed analytical model captures the response of sliding isolated two-story building model satisfactorily.

The experimental results of the fault normal Newhall 360 and Sylmar 360 excitations indicated essentially a similar response as in the passive high damping case (Sahasrabudhe 2002) and hence are not shown here due to lack of space.

In order to study the effect of change in the base mass on the response, experiments were performed with the base mass changed to 0.98 kN instead of 5.44 kN (Sahasrabudhe et al. 2000). Results are presented in Figs. 15 and 16 for: (1) El Centro, (2) Sylmar 90, and (3) Newhall 90. The relative base displacements in the two mass cases in the controlled case are similar in magnitude, i.e., base displacement remains virtually constant at higher table accelerations. However in the passive low and high damping cases, the response changes with the change in base mass. Particularly, largest base displacement occurs in the passive high damping case due to Newhall 90 (nearly 1 g) when compared to both passive low and controlled case. Hence, increasing damping does not necessarily result in a lower base displacement response. The controlled case is not influenced by the change in

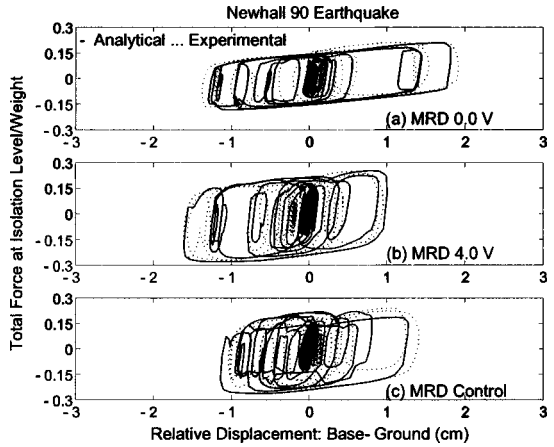


**Fig. 10.** Comparison of analytical and experimental total force-displacement loops for Newhall 90 excitation. (Note: Variation of force due to switching of magnetorheological damper in (c).)

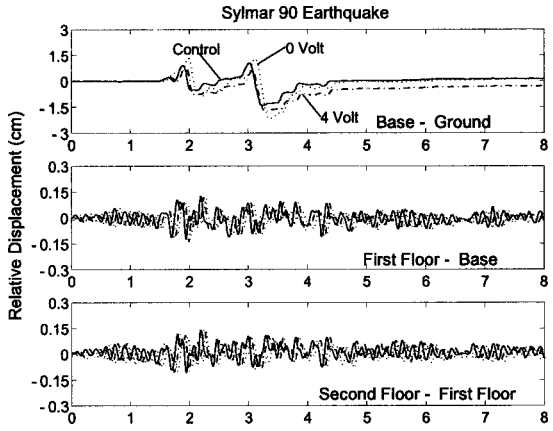


**Fig. 12.** Comparison of experimental displacement response under Sylmar 90

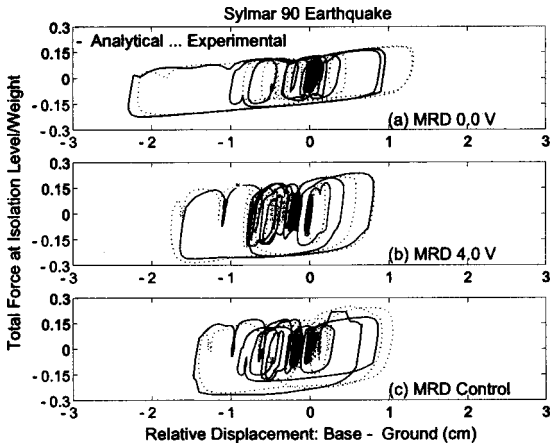


**Fig. 13.** Comparison of analytical and experimental total force-displacement loops to Sylmar 90 excitation. [Note: Variation of force due to switching of magnetorheological damper in (c).]

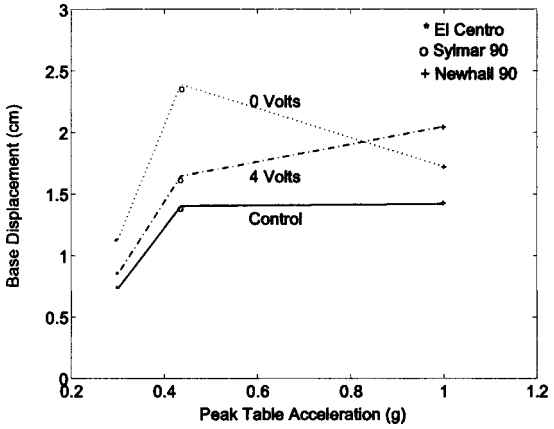


**Fig. 15.** Comparison of experimental peak relative base displacement for two-story model with 0.98 kN base

base mass; hence it is robust. As is evident from Fig. 16, the isolation level forces in the controlled case are lower than the passive high damping case.

Additionally, Kobe NS [0.65 g-80% and 0.816 g-100%), Kobe EW (0.62 g-100%), fault normal components Newhall 360 (0.59 g-100%), and Sylmar 360 (0.84 g-100%) were studied analytically (Sahasrabudhe 2002). Under Kobe NS excitation with 80% and 100% intensities, the controlled case gives the least relative base displacement response, when compared to the passive low and high damping cases, resulting in a total of 16% reduction in 80% intensity earthquake, and 24% reduction in 100% intensity earthquake. Under both the 80% and 100% intensity Kobe NS excitations, the controlled case also maintains isolation level forces, interstory drifts, and accelerations within bounds of the two passive cases. Thus, the developed control algorithm is effective under different earthquake intensities as well. In the Kobe EW case, the controlled response is similar to the passive high damping case.

From the analytical and experimental study, it is evident that the controlled case maintains the same or lower level of isolation force when compared to the passive high damping case. An obvious question arises as to whether it is possible to maintain the displacement reductions achievable by the passive high damping case with the corresponding total forces being close to the passive low damping case? In order to answer this question an analytical study is performed with MR damper switching between 0 to 2 V (instead of 1 to 4 V) based on the same Lyapunov controller. Results are presented in Table 3 for four earthquakes: (1) El Centro, (2) Sylmar 90, (3) Newhall 90, and (4) Kobe NS (80%). The results from Table 3 indeed reveal that the base displacements close to that of the passive high damping case can be achieved in the controlled case, while maintaining isolation level forces nearly the same as that of the passive low damping case. Such reductions are achieved with less damping variation—damping ratio varying between ~6% (0 V) and ~20% (2 V) as against ~6% (0 V), and ~45% (4 V).

In summary, it can be concluded that the semiactive controlled case reduces the base displacement further than the passive low and high damping cases, while maintaining isolation level forces lower than the passive high damping case, in fault-parallel earthquakes. It may be possible to reduce the response in fault normal earthquakes with better control algorithms than the one presented in this study.

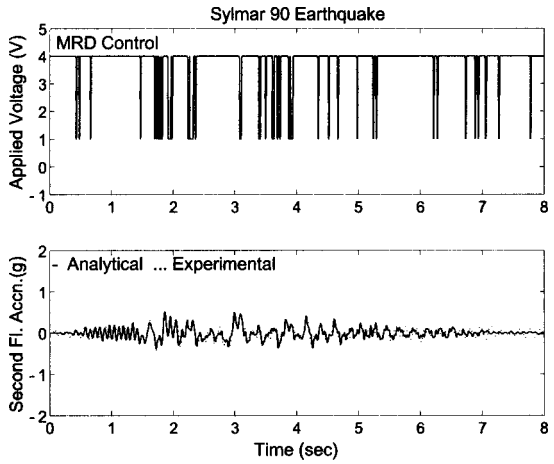


**Fig. 14.** Magnetorheological damper switching and comparison of analytical and experimental second floor acceleration time history response for Sylmar 90 earthquake

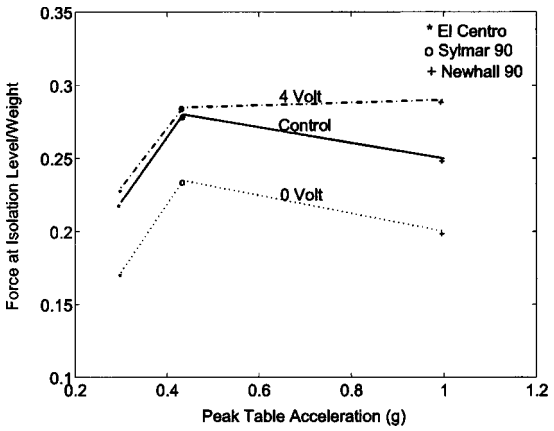


**Fig. 16.** Comparison of experimental peak isolation level force for the two-story model with 0.98 kN base

**Table 3.** Comparison of Analytical Response with Controller Switching between 0–2 V

| | Relative base displacement (cm) | | | Force at isolation level/weight | | |
|---|---|---|---|---|---|---|
| Earthquake | 0.0 V | 4.0 V | Control | 0.0 V | 4.0 V | Control |
| Sylmar 90 | 2.29 | 1.65 | 1.81 | 0.22 | 0.26 | 0.24 |
| Newhall 90 | 1.82 | 1.61 | 1.51 | 0.21 | 0.28 | 0.22 |
| El Centro | 0.94 | 0.65 | 0.84 | 0.16 | 0.24 | 0.2 |
| Kobe NS (80%) | 2.51 | 2.45 | 2.09 | 0.20 | 0.29 | 0.25 |

## Conclusions

The seismic response and performance of sliding isolated building with MR damper is evaluated analytically and experimentally. It is evident from the analytical and experimental study that the semiactive controlled case reduces the bearing displacements further than the passive low and high damping cases, while reducing isolation level forces when compared to the passive high damping case. The main conclusions of this study are:

- Passive high damping reduces base displacements but at the expense of increased isolation level forces and superstructure drifts.
- A MR damper with the developed control algorithm reduces bearing displacements further than the passive high and low damping cases, while maintaining the isolation level forces less than the passive high damping case. With the appropriate choice of damping levels, the MR damper can reduce base displacements similar to passive high damping case while reducing the isolation level forces to that of the passive low damping case.
- The semiactive controlled case also maintains the superstructure interstory drift and acceleration responses within bounds of the passive high and low damping cases.
- The proposed analytical model which incorporates hysteretic characteristics of sliding bearings and MR damper captures the response of the building model satisfactorily.

It is evident that the developed control algorithm is effective under fault-parallel components of the earthquakes considered in this study; the controlled response under fault-normal earthquakes is same as that of the passive high damping case. Since the results of analytical study are in good agreement with experimental results, the analytical model can be used for extensive analytical study to compute the response under various earthquakes and test different control algorithms. It may be possible to reduce the response in fault normal earthquakes with better control algorithms than the one presented in this study.

## Acknowledgments

Funding for this project provided by the National Science Foundation, NSF-CAREER Grant No. CMS-9996290, is gratefully acknowledged.

## References

Asher, J. W., Young, R. P., and Ewing, R. D. (1996). "Seismic isolation design of the San Bernardino county medical center replacement project." *Struct. Des. Tall Build.*, 5, 265–279.

Carlson, J. D., and Chrzan, M. J. (1994). "Magnetorheological fluid dampers, " U. S. Patent No. 5,277,281.

Gavin, H. P. (2001). "Control of seismically excited vibration using electrorheological materials and Lyapunov methods." *IEEE Trans. Autom. Control* 9(1), 27–36.

Gavin, H. P., Alhan, C., and Oka, N. (2003). "Fault tolerance of semiactive seismic isolation." *J. Struct. Eng.* 129(7), 922–932.

Hall, J. F., Heaton, T. H., Halling, M. W., and Wald, D. J. (1995). "Near-source ground motion and its effects on flexible buildings." *Earthquake Spectra* 11, 569–605.

Kelly, J. M. (1997). *Earthquake-resistant design with rubber*, 2nd Ed., Springer, N.Y.

Kelly, J. M. (1999). "The role of damping in seismic isolation," *Earthquake Eng. Struct. Dyn.* 28, 3–20.

Kurata, N., Kobori, T., Takahashi, M., Niwa, N., and Hiroshi, M. (1999). "Actual seismic response controlled building with semiactive damper." *Earthquake Eng. Struct. Dyn.* 28(11), 1427–1447.

Madden, G. J., Symans, M. D., and Wongprasert, N. (2002). "Experimental verification of seismic response of building frames with adaptive sliding base-isolation system." *J. Struct. Eng.* 128(8), 1037–1045.

Madden, G. J., Wongprasert, N., and Symans, M. D. (2003). "Analytical and numerical study of a smart sliding isolation system for seismic protection of buildings." *Comput. Aided Civ. Infrastruct. Eng.* 18, 19–30.

Makris, N. (1997). "Rigidity-plasticity viscosity: Can electrorheological dampers protect base isolated structures from near-source ground motions?" *Earthquake Eng. Struct. Dyn.* 26, 571–591.

Makris, N., and Chang, S. P. (2000). "Effect of viscous, viscoplastic, and friction damping in the response of seismically isolated structures." *Earthquake Eng. Struct. Dyn.* 29, 85–107.

Mills, R. S., Krawinkler, H., and Gere, J. M. (1979). "Model tests on earthquake simulators development and implementation of experimental procedures." *Rep. No. 39*, John A. Blume Earthquake Engineering Center, Stanford Univ., Stanford Calif.

Naeim, F., and Kelly, J. M. (1999). *Design of seismic isolated structures*, 1st Ed., Wiley, N.Y.

Nagarajaiah, S. (1994). "Fuzzy controller for structures with hybrid isolation system." *Proc., 2nd World Conference on Structural Control*, Wiley, N.Y., TA2:67-76.

Nagarajaiah, S., Reinhorn, A. M., and Constantinou, M. C. (1991a). "*3D-BASIS*: Nonlinear dynamic analysis of three-dimensional base isolated structures—Part II." *Rep. No. NCEER-91-0005*, National Center for Earthquake Engineering Research, SUNY, Buffalo, N.Y.

Nagarajaiah, S., Reinhorn, A. M., and Constantinou, M. C. (1991b). "Nonlinear dynamic analysis of 3D-base isolated structures." *J. Struct. Eng.*, 117(7), 2035–2054.

Nagarajaiah, S., Riley, M. A., and Reinhorn, A. M. (1993). "Control of sliding isolated bridges with absolute acceleration feedback." *J. Eng. Mech.*, 119(11), 2317–2332.

Nagarajaiah, S., and Sun, X. (2000), "Response of base isolated USC hospital building in Northridge Earthquake." *J. Struct. Eng.* 126(10), 1177–1186.

Nagarajaiah, S., and Sun, X. (2001). "Base-isolated FCC Building: Impact response during Northridge earthquake." *J. Struct. Eng.* 127(9), 1063–1074.

Narasimhan, S., and Nagarahaiah, S. (2005). "STFT algorithm for semiactive control of base isolated buildings with variable stiffness isolation systems subjected to near fault earthquakes." *Eng. Struct.*, 27, 514–523.

Ramallo, J. C., Johnson, E. A., and Spencer, B. F. (2002). "Smart base isolation systems." *J. Eng. Mech.* 128(10), 1088–1099.

Sahasrabudhe, S. (2002). "Semi-active control of sliding isolated buildings and bridges with variable stiffness and damping systems." PhD thesis, Rice Univ., Houston, Tex.

Sahasrabudhe, S. and Nagarajaiah, S.. (2005). "Semiactive control of sliding isolated bridges using MR dampers: An experimental and numerical study." *Earthquake Eng. Struct. Dyn.*, Published online January 31, 2005.

Sahasrabudhe, S., Nagarajaiah, S., and Hard, C. (2000). "Experimental study of sliding isolated buildings with smart dampers subjected to near-source ground motions." *Proc., Engineering Mechanics Conf., ASCE, EM 2000* (CD-Rom), Austin, Tex.

Spencer, B. F., Dyke, S. J., and Deoskar, H. S. (1998). "Benchmark problems in structural control: Part I—Active mass driver system." *Earthquake Eng. Struct. Dyn.* 27, 1127–1139.

Spencer, B. F., Dyke, S. J., Sain, M. K., and Carlson, J. D. (1997). "Phenomenological model of magnetorheological damper," *J. Eng. Mech.* 123(3), 230–238.

Spencer, B. F., and Nagarajaiah, S. (2003). "State of the art structural control." *J. Struct. Eng.* 129(7), 845–856.

Symans, M. D., and Constantinou, M. C. (1999). "Semiactive control systems for seismic protection of structures: A state of the art review." *Eng. Struct.* 21, 469–487.

Symans, M. D., and Kelly, S. W. (1999). "Fuzzy logic control of bridge structures using intelligent semi-active seismic isolation systems." *Earthquake Eng. Struct. Dyn.* 28(1), 37–60.

Wen, Y. K. (1976). "Method of random vibration of hysteretic systems." *J. Eng. Mech.*, 102(2), 249–263.

Yang, J. N., and Agrawal, A. K. (2002). "Semiactive hybrid control systems for nonlinear buildings against near-field earthquakes." *Eng. Struct.* 24, 271–280.

Yoshioka, H., Ramallo, J. C., and Spencer, B. F. (2002). " 'Smart' base isolation strategies employing magnetorheological dampers." *J. Struct. Eng.* 128(5), 540–551.

Zhang, Y., and Iwan, W. D. (2002). "Protecting base-isolated structures from near-field ground motion by tuned interaction damper," *J. Eng. Mech.* 128(3), 287–295.